ANALYSIS OF FREE SURFACE MOMENTUM AND ENERGY TRANSPORT IN POROUS MEDIA

S. C. Chen and K. Vafai
Department of Mechanical Engineering,
Ohio State University, Columbus, Ohio 43210, USA

The phenomenological analysis of free surface transport through porous media is presented. A finite difference scheme using the Marker and Cell (MAC) method is employed to investigate the momentum and energy transport in a porous channel involving free surface transport phenomena. To the best of the authors' knowledge, this is the first investigation of free surface momentum and energy transport through porous media and is also the first application of the MAC method for exploring the free surface transport phenomena in a porous medium. Limiting case comparisons are made with an existing analytical solution for flow through a channel filled with a porous medium. Excellent agreement is obtained for both the temperature and velocity distributions. Temporal free surface positions are also compared and verified against an existing analytical solution. A detailed analysis of the encroachment of two immiscible fluids in a porous channel using Darcy's model is presented. The effects of pressure differences and permeabilities on free surface transport through a porous medium are investigated. The effect of the free surface transport in porous media on the energy transfer is also explored.

INTRODUCTION

The prediction of the fluid interface displacement has become increasingly important in some manufacturing processes, such as injection molding and die filling. Related studies have been performed in the oil industry to understand the simultaneous flow of oil, water, and gas in porous strata during the production of oil from oil fields. The study of linear encroachment was done by Muskat [1], where a one-dimensional Darcy's flow model was used to investigate two fluids moving in a narrow channel. A comprehensive analytical study was done by Srinivasan and Vafai [2] to obtain a further understanding and better prediction of the interface for the linear encroachment in a system of two immiscible fluids in which the boundary and inertial effects were accounted for. In this work, a two-dimensional investigation of the encroachment of an immiscible fluid in a porous channel is performed. One fluid initially saturates the porous channel, and the pressure field at the free surface is assumed to be fixed. The approach developed by Vafai and Chen [3] was employed in the present study. The finite difference method (FDM) is used to solve the governing equations, and the Marker and Cell (MAC) method is employed to predict the free surface motion.

Received 5 June 1995; accepted 9 October 1995.
Support from the EES Corporation during the course of this study is greatly appreciated.
Address correspondence to Dr. K. Vafai, Department of Mechanical Engineering, The Ohio State University, 206 W. 18th Avenue, Columbus, OH 43210-1107, USA.

Numerical Heat Transfer, Part A, 29:281–296, 1996

1040–7782/96 $12.00 + .00

NOMENCLATURE

Da	Darcy Number $[= K/(H^2\theta)]$	T_w	channel wall temperature
F	inertial constant	T_∞	ambient temperature
h	heat transfer coefficient	u	x component velocity
H	one half of channel height	u_∞	channel centerline velocity
k_e	effective thermal conductivity of the porous matrix	v	y component velocity
		x_i	initial location of the fluid
K	permeability	x_o	free surface front location
L	horizontal extent of the channel	α_m	effective thermal diffusivity
Nu	Nusselt number $\{= [q/(T_w - T_m)](2H/k_e)\}$	Δp	pressure difference across the encroaching fluid field region, N/m^2
p	pressure	ε	mobility ratio $(= \mu_2/\mu_1)$
p_e	entrance pressure	θ	porosity of the porous medium
p_∞	ambient pressure	μ_f	fluid viscosity
q	wall heat flux	μ_1	residing fluid viscosity
Re_K	Reynolds Number $(= u_D\sqrt{K}/\nu_f)$	μ_2	encroaching fluid viscosity
T_e	entrance temperature	ν_f	kinematic viscosity
T_m	bulk mean temperature	ρ_f	fluid density

The MAC method, originally developed at the Los Alamos Laboratory by Harlow and Welch [4], solves the incompressible transient flow equations using primitive variables, namely, pressure and velocity components, in a staggered grid system. Eulerian fluid cells and the coordinates of a set of marker particles that move with the fluid were used to track the free surface position. Several applications were studied based on the early version of the MAC method. A technique including surface stress condition and curvature effects was introduced by Daly and Pracht [5]. Hirt and Shannon [6], in their study of a viscous bore, investigated the limits of the original version of the MAC method. With a simple modification, it is possible to approximate the complete normal stress condition, and this modification was shown to have a pronounced effect on some low-Reynolds-number flows. Furthermore, modifications on the details of the numerical method, such as interpolation schemes and more exact application of the pressure boundary condition, were made by Chan and Street [7] in their numerical study of finite amplitude water waves. Hirt et al. [8] incorporated the complete free surface stress conditions into a numerical technique in their study of a viscous bore. Frederiksen and Watts [9] studied entrainment of fluid by a vertically moving plate from a bath of fluid of finite depth and the consequent formation of a thin film of fluid on the plate using an iterative finite element technique. Later, an experimental investigation of free surface transport and subsequent bifurcation and adhesion for a hollow ampule was done by Chen and Vafai [10].

In the present study, a constant pressure field at the interface is accomplished by assuming a very low viscosity for the region without any fluid. This assumption enables us to perform direct comparison with an existing analytical solution by Srinivasan and Vafai [2]. The analytical solution by Srinivasan and Vafai [2] is modified with the interface starting from a prespecified location to facilitate comparative analysis. This is the first time the MAC method is applied to flow in a porous channel. Excellent agreement was obtained in comparisons with the exact solution of Vafai and Kim [11] and the analytical solution of Srinivasan and Vafai [2].

ANALYSIS

Figure 1 presents a schematic diagram of the problem. There is a specified fluid "2" initially residing in the porous channel, and the pressure at the interface is fixed throughout the simulation. A modification of the analytical solution of Srinivasan and Vafai [2] is made to account for the initial position of the interface. A very low viscosity value is assumed for the area without any fluid, so direct comparison of the temporal free surface distributions can be accomplished.

Governing Equations

As shown in the work of Vafai and Tien [12], the velocity field develops in a relatively short distance of the order of $K\bar{u}\nu^{-1}$ from the entrance. Therefore, since the convective terms are important only within this short length, they are neglected. Time dependent terms are also ignored in the momentum equation because, based on the work of Vafai and Tien [13], it has been shown that the steady state momentum field is established in a very short time period. Without the convective and time dependent terms, and assuming local thermal equilibrium, the continuity, momentum, and energy equations are obtained using the local volume averaging technique.

Continuity equation

$$\frac{\partial u}{\partial x} + \frac{\partial v}{\partial y} = 0 \tag{1}$$

Momentum equation

$$-\frac{\theta}{\rho_f}\bar{\nabla}p_f + \frac{\mu_f}{\rho_f}\nabla^2 U - \left(\frac{\mu_f \theta U}{K\rho_f} + \frac{FU\theta|U|}{\sqrt{K}}\right) = 0 \tag{2}$$

Energy equation

$$u\frac{\partial T}{\partial x} + v\frac{\partial T}{\partial y} = \alpha_m\left(\frac{\partial^2 T}{\partial^2 x} + \frac{\partial^2 T}{\partial^2 y}\right) \tag{3}$$

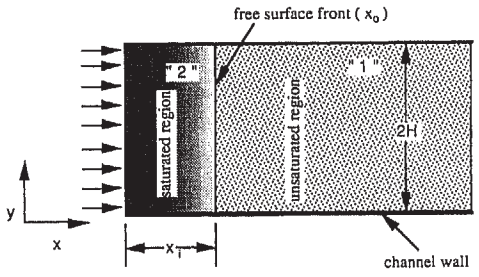

Figure 1. Free surface transport through a porous channel.

In the above equations, p_f represents the pressure read off a pressure gage, as the gage actually measures the average pressure inside the fluid, μ_f is fluid viscosity, ρ_f is fluid density, K is the permeability of the porous medium, θ is porosity, F is the inertial constant, as defined by Vafai and Tien [13], and α_m is the effective thermal diffusivity of the porous channel.

The experimental procedure for determining the value of K and F is described by Vafai and Tien [13]. The typical values of K and the given functional dependence of F can be deduced from a number of empirical results, such as those of Muskat [1] and Koh et al. [14]. In the present study, both x and y momentum equations are solved even though the pressure gradient in the y direction is negligible, as shown by Vafai [15]. However, the flow is primarily driven by the pressure gradient in the axial direction.

The boundary, initial, and interface conditions required to solve the governing equations are expressed as follows.

Boundary conditions

$$p = p_e \qquad v = 0 \qquad T = T_e \qquad x = 0 \tag{4}$$

$$p = p_\infty \qquad \frac{\partial u}{\partial x} = 0 \qquad -k_e \frac{\partial T}{\partial x} = h(T - T_\infty) \qquad x = x_0 \tag{5}$$

$$u = v = 0 \qquad T = T_w \qquad y = 0 \qquad y = 2H \tag{6}$$

Initial condition

$$u = v = 0 \qquad T = T_\infty \qquad x = x_i \qquad t = 0 \tag{7}$$

where x_0 represents the free surface position, p_e the entrance pressure, p_∞ the ambient pressure, T_e the entrance temperature, T_w the wall temperature, T_∞ the ambient temperature, x_i the initial position of the free surface, h the heat transfer coefficient, and k_e the effective thermal conductivity.

The general form of the initial condition for the free surface location is based on practical applications such as in injection molding. It is based on some fluid residing in the porous channel where a high pressure is applied at the entrance of the channel. In order to make appropriate comparisons with the analytical solution presented by Srinivasan and Vafai [2], the analytical solution is modified to account for the existing encroaching fluid. The derivation of the modified solution is somewhat complicated, and here we present only the final form as

$$\frac{x_0}{L} = \frac{1 - \sqrt{1 + 2(1-\varepsilon)\left\{(-K/\mu_1\theta)(\Delta p/L^2)t + [(1-\varepsilon)/2](x_i/L)^2 - (x_i/L)\right\}}}{(1-\varepsilon)} \tag{8}$$

where x_i represents the initial location of the encroaching fluid.

Numerical Methodology

The finite difference formulation for the governing equations is similar to that presented in the work by Vafai and Chen [3]. A brief description of the discretization of the governing equation is presented as follows.

x momentum

$$\left[-\frac{\theta}{\rho_f}\frac{\partial p_f}{\partial x}+\frac{\mu_f}{\rho_f}\nabla^2 u-\left(\frac{\mu_f\theta u}{K\rho_f}+\frac{Fu\theta|U|}{\sqrt{K}}\right)\right]=0 \tag{9}$$

y momentum

$$\left[-\frac{\theta}{\rho_f}\frac{\partial p_f}{\partial y}+\frac{\mu_f}{\rho_f}\nabla^2 v-\left(\frac{\mu_f\theta v}{K\rho_f}+\frac{Fv\theta|U|}{\sqrt{K}}\right)\right]=0 \tag{10}$$

Equations (9) and (10) can be written as

$$-\frac{\theta}{\rho_f}\frac{\partial p_f}{\partial x}+f(x,y)=0 \tag{11}$$

$$-\frac{\theta}{\rho_f}\frac{\partial p_f}{\partial y}+g(x,y)=0 \tag{12}$$

where $f(x, y)$ and $g(x, y)$ are defined as

$$f(x,y)=\frac{\mu_f}{\rho_f}\nabla^2 u-\left(\frac{\mu_f\theta u}{K\rho_f}+\frac{Fu\theta|U|}{\sqrt{K}}\right) \tag{13}$$

$$g(x,y)=\frac{\mu_f}{\rho_f}\nabla^2 v-\left(\frac{\mu_f\theta v}{K\rho_f}+\frac{Fv\theta|U|}{\sqrt{K}}\right) \tag{14}$$

Cross differentiating Eqs. (11) and (12) will result in the following equation:

$$\overline{\nabla}^2 p_f=\frac{\rho_f}{\theta}\left(\frac{\partial f(x,y)}{\partial x}+\frac{\partial g(x,y)}{\partial y}\right) \tag{15}$$

The successive overrelaxation (SOR) method is employed in solving the discretized momentum and pressure equations. As mentioned earlier, the MAC method is utilized to track the temporal free surface position. During the process, extrapolation of the velocity fields in the empty cells is required to carry out the numerical iteration of the momentum and pressure equations. Calculation of the marker particle velocities is accomplished based on the obtained velocity field to move the free surface position as the process proceeds. An implicit scheme is used to solve the energy equation. The basic aspects of the above-mentioned schemes are presented in the work of Vafai and Chen [3]. The implementation of the present numerical scheme will not be presented here for the sake of brevity.

RESULTS AND DISCUSSION

Comparison of the fully developed velocity and temperature fields produced by the method described above with the exact solution by Vafai and Kim [11] is presented in Figures 2*a* and 2*b*. The fully developed velocity and temperature fields were obtained by solving the governing equations for the configuration shown in Figure 1. As shown in Figure 2*a*, for $K = 8.0 \times 10^{-4}$ m^2, the boundary thickness is about 3% of the channel width for an 80% porosity. This is consistent with the results pointed out by Vafai and Tien [12] that the boundary layer thickness is of the order of $(K/\theta)^{1/2}$. In order to capture the momentum boundary layer, a variable grid size is employed with a very fine grid structure close to the wall. The difference between the current numerical result and that of the analytical solution given by Vafai and Kim [11] is less than 0.4%. Referring to Figure 2*a*, the two curves coincide on top of each other. The same accuracy is obtained for the temperature field in Figure 2*b*, with the difference being less than 0.4%.

Figure 3*a* depicts the axial distribution of the Nusselt number for a constant wall temperature for the case presented in Figure 2 when Darcy's model is employed for the momentum equations. When the porous matrix is sandwiched between two parallel plates, the corresponding Nusselt number is 6.00 for a constant wall heat flux, as indicated by Vafai and Kim [11]. This is indeed what is obtained in Figure 3*a*, further confirming the accuracy of our numerical scheme. Three cases with $K = 8.0 \times 10^{-5}$, 8.0×10^{-8}, and 8.0×10^{-11} m^2 are investigated and compared with an existing analytical solution. These cases are chosen to cover a reasonable range of permeabilities employed in practical applications. Referring to Figures 3*b*–3*d*, the free surface front comparisons versus the analytical work of Srinivasan and Vafai [2] show excellent agreement, further confirming the robustness of the employed numerical scheme.

Next, the effects of variation in the Reynolds number based on permeability, Re_K, while Darcy's number is held constant are investigated for the free surface transport through porous media. Three cases, designated case 1, case 2, and case 3, are studied using $\mathrm{Da} = 1.0 \times 10^{-6}$. Pressure differences of 5.0×10^5 N/m^2 for

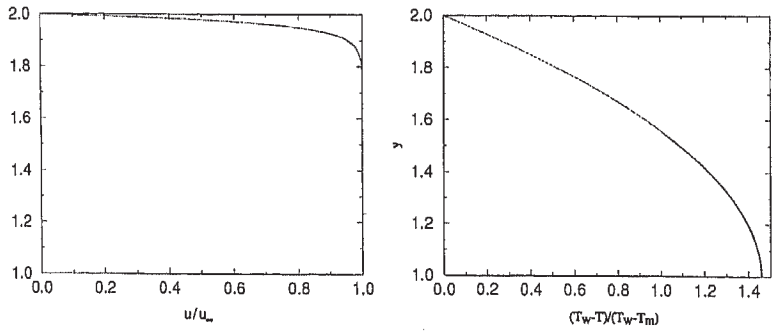

Figure 2. Comparison of fully developed (*a*) velocity and (*b*) temperature fields with the analytical solutions of Vafai and Kim [11] for $K = 8.0 \times 10^{-4}$ m^2.

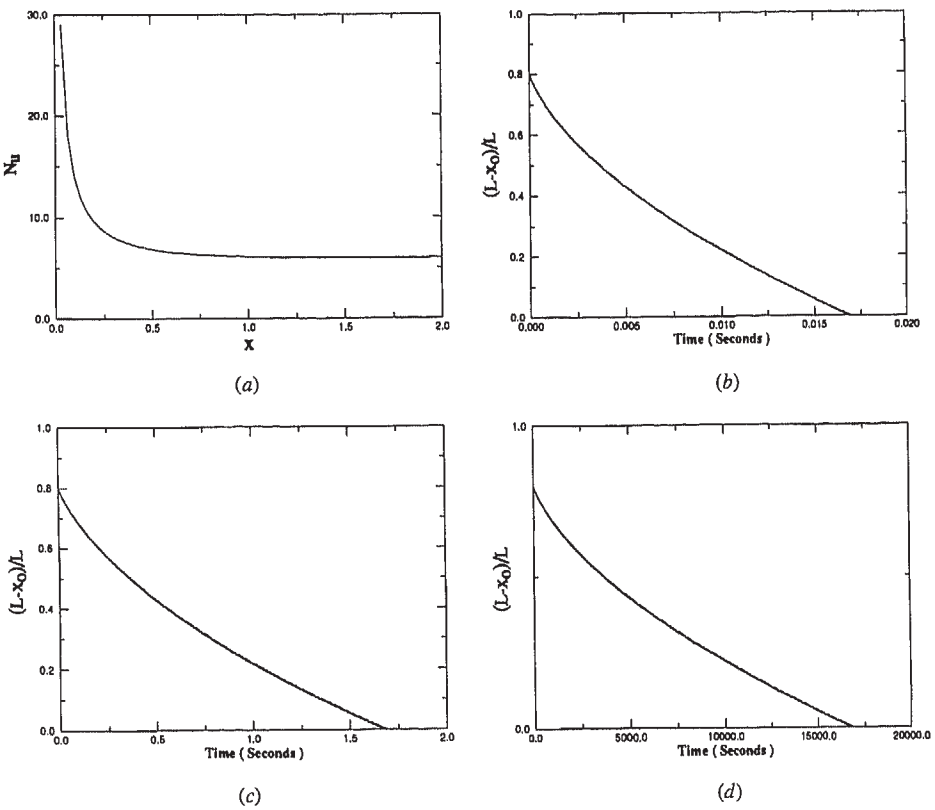

Figure 3. (*a*) Fully developed axial Nusselt number distribution. Comparison of temporal free surface distribution with analytical solutions by Srinivasan and Vafai [2] for (*b*) Da = 1.0×10^{-4} and $\mathrm{Re}_K = 5.72 \times 10^{-1}$, (*c*) Da = 1.0×10^{-7} and $\mathrm{Re}_K = 1.81 \times 10^{-4}$, and (*d*) Da = 1.0×10^{-10} and $\mathrm{Re}_K = 5.72 \times 10^{-10}$.

case 1, 5.0×10^6 N/m^2 for case 2, and 5.0×10^7 N/m^2 for case 3 are applied, and these correspond to $\mathrm{Re}_K = 5.72 \times 10^{-4}$, 5.72×10^{-3}, and 5.72×10^{-2}, respectively. The temporal free surface distributions for cases 1, 2, and 3 are presented in Figure 4. Figures 5–7 illustrate the temperature distributions at selected time frames for each case. The pressure difference for the saturated portion is assumed to be constant throughout the process, and the encroaching fluid occupies a portion of the channel initially.

Referring to Figure 4, it takes about 1.7 s for case 1, 0.17 s for case 2, and 0.017 s for case 3 for the encroaching fluid to fill up the entire channel. The required time is directly proportional to the applied pressure difference for each case. This can be explained on the basis of the momentum transport equation. First, it should be noted that the temporal location of the free surface front is obtained on the basis of the temporal free surface velocity. Next, referring to Darcy's law, for cases 1–3, it can be seen that viscosity and permeability are identical, resulting in a velocity that is proportional to the applied pressure

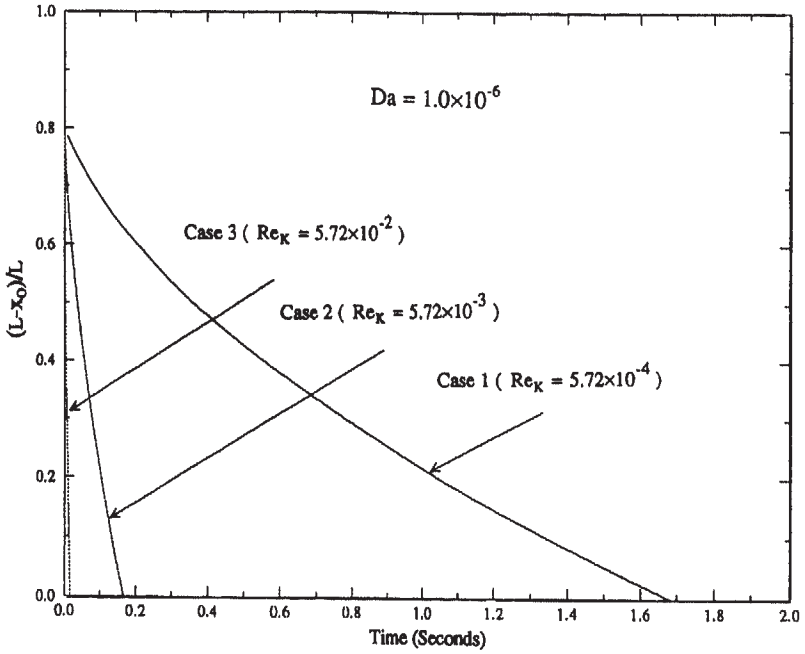

Figure 4. Temporal free surface distributions using constant Darcy number.

difference. Referring to Figure 4, a larger pressure difference results in a shorter time in which the encroaching fluid fully saturates the porous channel.

The temperature contours at three time frames are presented in Figures 5, 6, and 7 for cases 1, 2, and 3. These contours show the impact of the flow field on the energy transport for different Re_K (different applied pressure differences). Figures 5*a*, 5*b*, and 5*c* illustrate the temperature contours at times equal to 0.5, 1.0, and 1.5 s. Referring to Figure 5, the temperature contours are symmetrical with respect to the centerline of the channel. A temperature value higher than the wall temperature is assumed for the encroaching fluid relating to a case where the hot fluid is injected into a cold porous channel. As shown in Figure 5*a*, at $t = 0.5$ s, the temperature of the encroaching fluid decreases as the heat is dissipated through the wall. The temperature reduction is larger at the wall region than at the center region due to larger losses near the wall region. As shown in Figure 5*b*, the temperature distribution close to the entrance area reduces at $t = 1.0$ s because more fluid is available to conduct heat through the channel wall. Referring to Figure 5*c* at $t = 1.5$ s, the channel is almost saturated with encroaching fluid, and the temperature reduces more for the entrance area with more heat conduction through the channel wall than at an earlier stage.

Figures 6*a*–6*c* present the temporal temperature contours at $t = 0.05$, 0.1, and 0.15 s for case 2 and with the same temporal free surface locations as case 1. Examining Figures 5 and 6, it can be seen that the temperature contours for case 2 are very close to those of case 1. This phenomenon can be explained as follows.

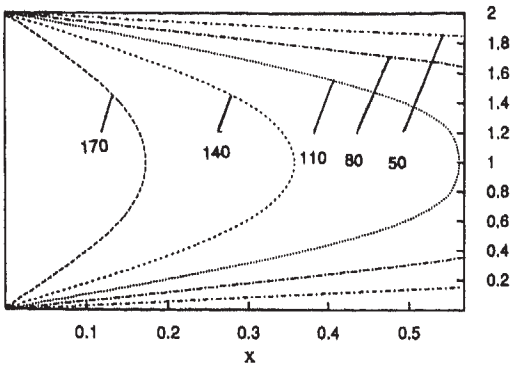

(*a*)

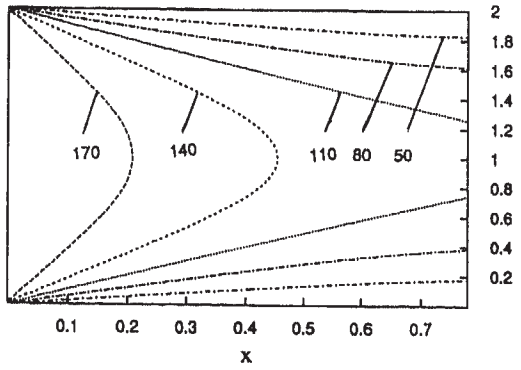

(*b*)

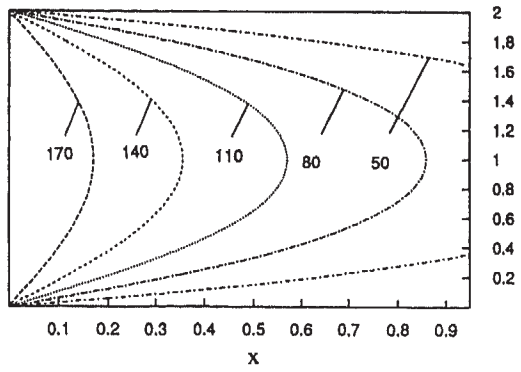

(*c*)

Figure 5. Temporal temperature (in degrees Celsius) distributions for case 1, $\mathrm{Re}_K = 5.72 \times 10^{-4}$ at (*a*) $t = 0.5$ s, (*b*) $t = 1.0$ s, (*c*) $t = 1.5$ s.

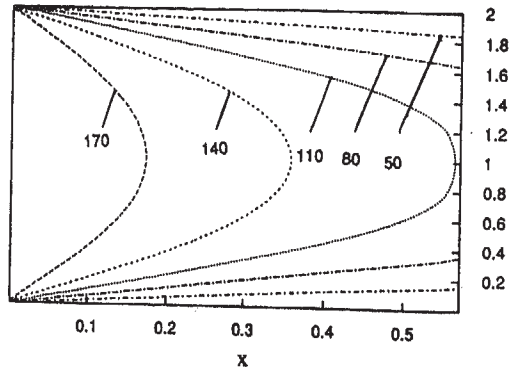

(*a*)

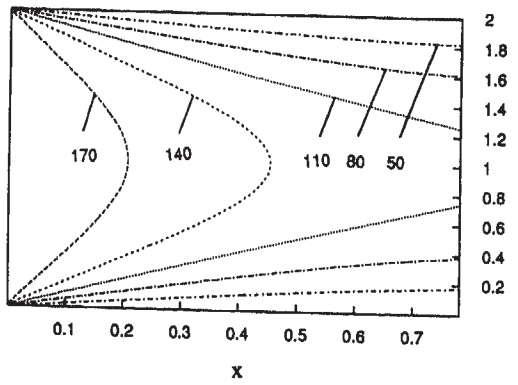

(*b*)

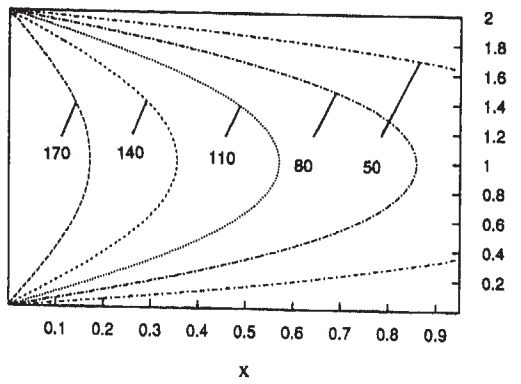

(*c*)

Figure 6. Temporal temperature (in degrees Celsius) distributions for case 2, $\mathrm{Re}_K = 5.72 \times 10^{-3}$ at (*a*) $t = 0.05$ s, (*b*) $t = 0.1$ s, and (*c*) $t = 0.15$ s.

Referring to Eq. (3), with the same physical domain and boundary conditions, the only factor resulting in different temperature distributions is due to the convective terms. However, at low Re flow such as in cases 1 and 2, the diffusive terms are far more dominant than the convective terms, resulting in very close temperature contours.

Figures 7*a*–7*c* present the temporal temperature contours for case 3 at the same free surface locations as case 1 and case 2 but at $t = 0.005$, 0.01, and 0.015 s. In comparison with Figures 5 or 6, the temperature contours in Figure 7 have been affected due to a more significant impact of convective heat transfer, which is in turn, related to the larger value of pressure difference. The differences can be more clearly seen at the centerline area as opposed to the wall region. This is due to the larger temperature gradients that are experienced close to the wall, resulting in a more dominant diffusive effect. As the process proceeds, the saturated portion of the channel increases, and the velocity decreases. Therefore for larger times, the impact of the convective terms becomes less significant due to the reduction of velocity. Referring to Figures 6 and 7 differences early on between cases 2 and 3 can be detected visually; however, at later times, the differences become less detectable.

Figure 8 presents the temporal free surface distributions for three cases, designated as cases 4, 5, and 6, using the same Re. In order to maintain constant Re_K defined as $u_D\sqrt{K}/\nu_f$, Da and pressure difference are varied for each case. Permeabilities of 8.0×10^{-5}, 8.0×10^{-6}, and 8.0×10^{-7} m^2 and pressure differences of 5.0×10^5, 1.58×10^7, and 5.0×10^8 N/m^2 are employed for cases 4, 5, and 6 to obtain the same Re_K. As shown in Figure 8 to fully saturate the porous channel, a time of 0.017 s is required for case 4, 0.0053 s for case 5, and 0.0017 s for case 6. As indicated earlier, the required time for fully saturating the channel is determined mainly by Darcy's velocity—the lower the velocity, the more time is consumed for the filling process. Darcy's velocity is about 3 times higher for case 6 than for case 5, and 10 times higher than for case 4. Therefore case 6 takes the least amount of time to fully saturate the porous channel, as shown in Figure 8.

Figures 9*a*–9*c* illustrate the temperature contours at $t = 0.001$ s for cases 4, 5, and 6. As shown in Figures 9*a*, for case 4, only a small portion of the channel is saturated and the impact of the convective terms is quite significant. Furthermore, the core region is able to maintain the entrance temperature field due to the prominence of the convective heat transfer. Comparing Figure 9 to Figure 6, it becomes clear that the core and mean bulk temperature at each cross section for cases 4, 5, and 6 are larger than for cases 1, 2, and 3. Again, this is due to the more prominent effect of the convective heat transfer for cases 4, 5, and 6.

Figure 10 displays the inertial effects on the temporal free surface position curves at three different Re. It can be seen that for applications such as groundwater flow and in injection molding, where the Re_K is usually small, inertial effects are almost negligible. However, for those applications that involve high permeabilities and medium or higher Re_K, the inertial effects can be quite significant. These results are consistent with the observations made by Vafai and Tien [12]. Neglecting the inertial effect could result in overprediction of the free surface front because the additional drag due to the inertial effects reduces the speed of the free

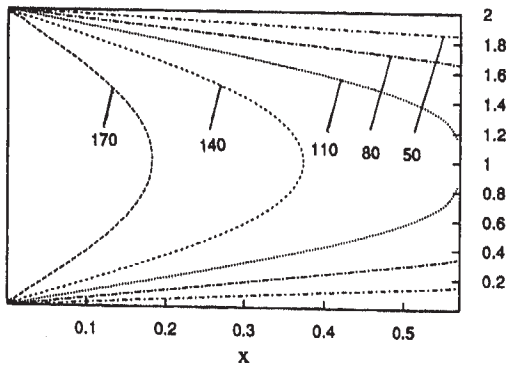

(*a*)

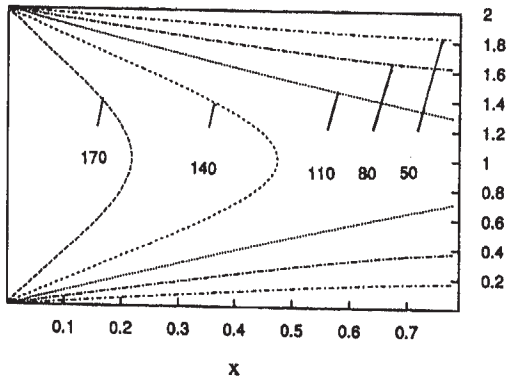

(*b*)

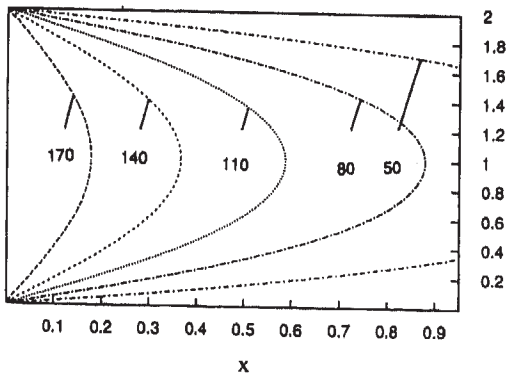

(*c*)

Figure 7. Temporal temperature (in degrees Celsius) distributions for case 3, $\mathrm{Re}_K = 5.72 \times 10^{-2}$ at (*a*) $t = 0.005$ s, (*b*) $t = 0.01$ s, and (*c*) $t = 0.015$ s.

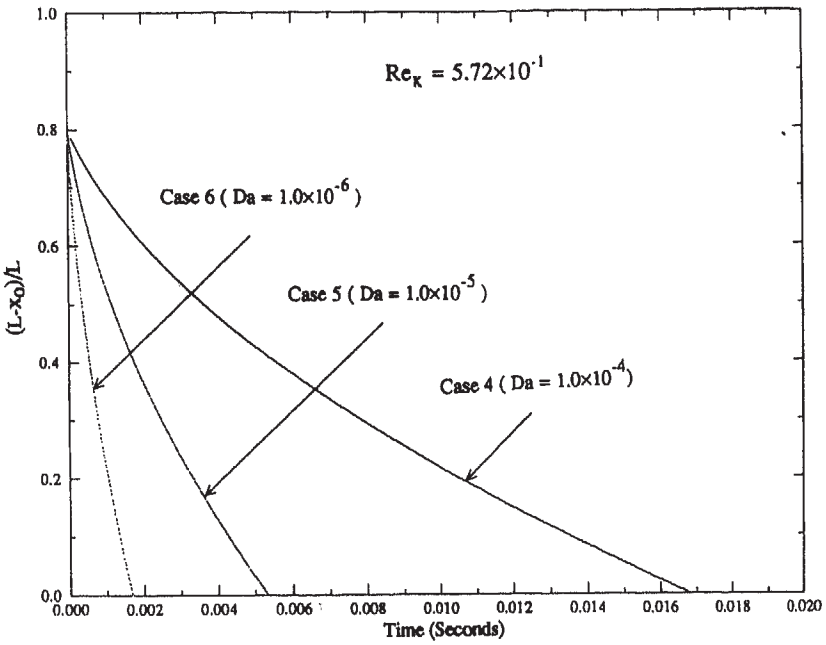

Figure 8. Temporal free surface distributions using constant Reynolds number.

surface front. As was shown in the work of Vafai and Kim [11], the impact of the inertial effects on the velocity field also becomes very significant at higher Da. The cited observations can be clearly seen in Figure 10, where for larger Re_K it takes more time for the free surface front to reach the end of the channel where the inertial effects are taken into account. For smaller Re_K the inertial effects diminish, as can be seen in Figures 10*b* and *c*. The difference in temporal free surface positions becomes almost negligible when Re is less than unity, as depicted in Figure 10*c*. These conclusions are consistent with those obtained in the work of Vafai and Tien [12] regarding the inertial effects on the general flow field.

CONCLUSIONS

A phenomenological analysis of free surface transport through porous media is presented. To the best of our knowledge, this is the first investigation of free surface momentum and energy transport through porous media as well as the first application of the Marker and Cell method to investigate the free surface transport phenomena in a porous medium. Excellent agreement is observed when limiting cases of the present results are compared with existing analytical results. Important observations are made regarding the time required for the encroaching fluid to fill up a channel for different permeabilities of the porous matrix. For example, it is observed that diffusive heat transfer is significantly more dominant than convective

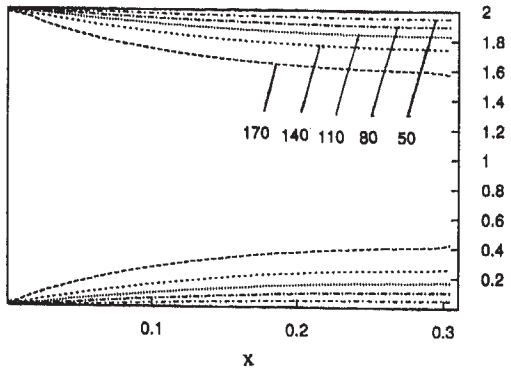

(*a*)

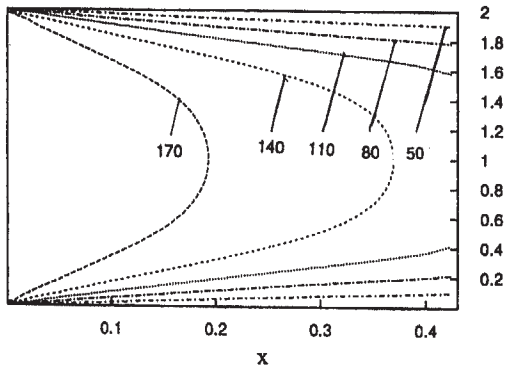

(*b*)

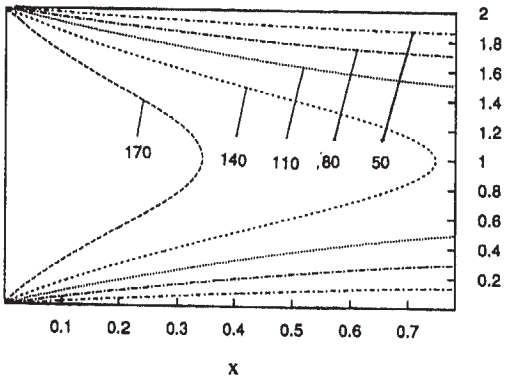

(*c*)

Figure 9. Temporal temperature (in degrees Celsius) distribution at $t = 0.001$ s for (*a*) case 4, (*b*) case 5, and (*c*) case 6.

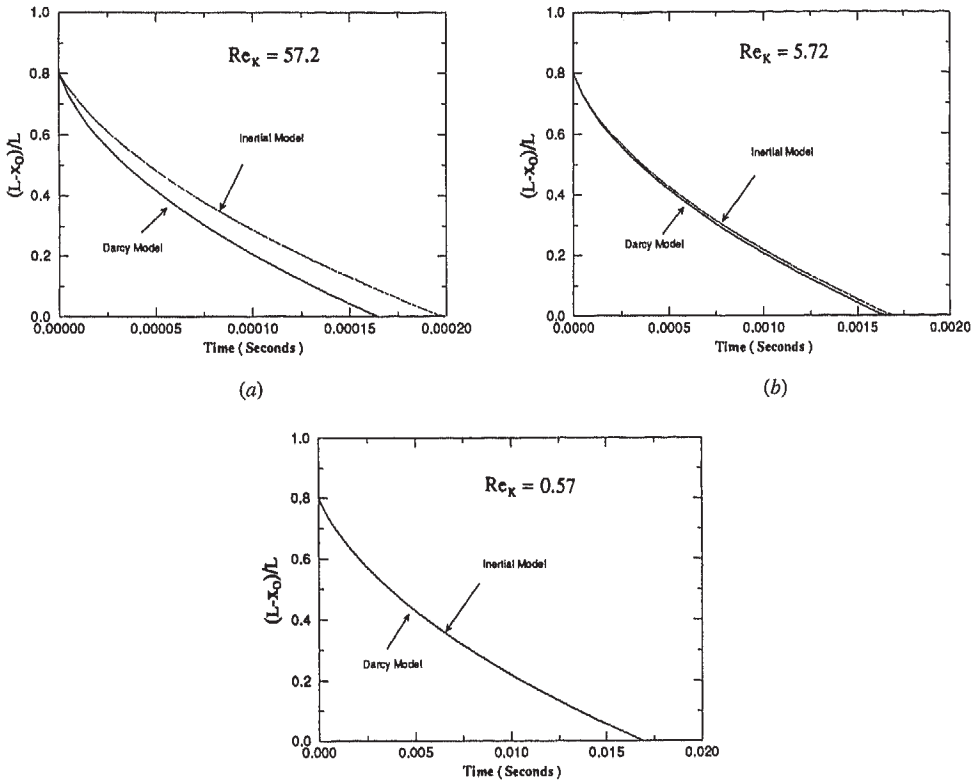

Figure 10. Comparison of temporal free surface positions with and without inertia terms for (*a*) $Re_K = 57.2$, (*b*) $Re_K = 5.72$, and (*c*) $Re_K = 0.57$.

heat transfer for free surface transport through porous media. The current work constitutes a rigorous investigation of free surface momentum and energy transport through porous media covering such applications as the injection molding process. It also forms a foundation for further understanding of flow and heat transfer characteristics of free surface transport through porous media.

REFERENCES

1. M. Muskat, *The Flow of Homogeneous Fluids Through Porous Media*, 1st ed., Edwards, Ann Arbor, Mich., 1937.
2. V. Srinivasan and K. Vafai, Analysis of Linear Encroachment in Two-Immiscible Fluid Systems in a Porous Medium, *J. Fluids Eng.*, vol. 116, pp. 135–139, 1994.
3. K. Vafai and S. C. Chen, Analysis of Free Surface Transport Within a Hollow Glass Ampule, *J. Numer. Heat Transfer Part A*, vol. 22, pp. 21–49, 1992.

4. F. H. Harlow and J. E. Welch, Numerical Calculation of Time-Dependent, Viscous, Incompressible Flow of Fluid with Free Surface, *Phys. Fluids*, vol. 8, pp. 2182–2189, 1965.
5. B. J. Daly and W. E. Pracht, Numerical Study of Density-Current Surge, *Phys. Fluids*, vol. 11, pp. 15–30, 1968.
6. C. W. Hirt and J. P. Shannon, Free-Surface Stress Condition Incompressible-Flow Calculations, *J. Comput. Phys.*, vol. 2, pp. 403–411, 1968.
7. R. K.-C. Chan and R. L. Street, A Computer Study of Finite Amplitude Water Waves, *J. Comput. Phys.*, vol. 6, pp. 68–94, 1970.
8. C. W. Hirt, J. L. Cook, and T. D. Butler, A Lagrangian Method for Calculating the Dynamics of an Incompressible Fluid with Free Surface, *J. Comput. Phys.*, vol. 5, pp. 103–124, 1970.
9. C. S. Frederiksen and A. M. Watts, Finite-Element Method for Time-Dependent Incompressible Free Surface Flow, *J. Comput. Phys.*, vol. 39, pp. 282–304, 1981.
10. S. C. Chen and K. Vafai, An Experimental Investigation of Free Surface Transport, Bifurcation and Adhesion Phenomena as Related to a Hollow Glass Ampule and a Metallic Conductor, *J. Heat Transfer*, vol. 114, pp. 743–751, 1992.
11. K. Vafai and S. J. Kim, Forced Convection in a Channel Filled with a Porous Medium: An Exact Solution, *J. Heat Transfer*, vol. 111, pp. 1103–1106, 1989.
12. K. Vafai and C. L. Tien, Boundary and Inertia Effects on Flow and Heat Transfer in Porous Medium, *Int. J. Heat Mass Transfer*, vol. 24, pp. 195–203, 1981.
13. K. Vafai and C. L. Tien, Boundary and Inertial Effects on Convective Mass Transfer in Porous Media, *Int. J. Heat Mass Transfer*, vol. 25, pp. 1183–1190, 1982.
14. J. C. Koh, J. C. Dutton, B. A. Benson, and A. Fortini, Friction Factor for Isothermal and Nonisothermal Flow Through Fibrous Porous Media, *J. Heat Transfer*, vol. 99C, pp. 367–373, 1977.
15. K. Vafai, Convective Flow and Heat Transfer in Variable-Porosity Media, *J. Fluid Mech.*, vol. 147, pp. 233–259, 1984.